Can We Estimate Air Density of the Thermosphere with CubeSats?

Raphael F. Garcia,* Zimo R. Sibbing,† and Adriaen Van Camp‡
ISAE-SUPAERO, University of Toulouse, 31400 Toulouse, France

DOI: 10.2514/1.A34324

The measurement of air density in the Earth's thermosphere has a wide range of scientific applications from space weather to upper atmosphere dynamics, but also technical applications from satellite control to predictions of atmospheric reentry of space debris. This study models the torques applying on a three-unit CubeSat in low Earth orbit to infer the capability of such platforms to measure the air density along their orbit. Realistic noise levels of available CubeSat components are used, and sensitivity to the various noise sources is presented. The precise knowledge of the spacecraft attitude, angular acceleration, residual magnetic dipole, and center of gravity is critical to allow proper air density retrieval. Winds in the thermosphere also have a significant impact on the thermosphere density retrieval, suggesting that this parameter can also be constrained. Attitude control is not necessary if the attitude itself is properly known. The application to the EntrySat CubeSat predicts that such retrieval is possible at altitudes lower than 200 km with errors lower than 30%. The air density retrieval from CubeSat platforms will open new capabilities to infer upper atmosphere dynamics.

Nomenclature

A, A_i	=	area (indexed), m^2
A_{ref}	=	reference Area, m^2
a	=	Earth albedo, 0.367
$\boldsymbol{B}$	=	magnetic field, $[3 \times 1]$, T
$C_{D,i,j}$	=	drag coefficient (indexed)
$C_{L,i,j}$	=	lift coefficient (indexed)
$\boldsymbol{C}_{r,i}$	=	radiation pressure coefficient (indexed), $[3 \times 1]$
c	=	speed of light, $2.99792458 \cdot 10^8$ m/s^2
$\hat{\boldsymbol{c}}$	=	unit vector along coil axis, $[3 \times 1]$
d	=	time, days
E	=	error
E_{rel}	=	relative error
F	=	visibility factor
$\boldsymbol{F}$, $\boldsymbol{F}_i$	=	force (indexed), $[3 \times 1]$
g	=	gravitational acceleration, m/s
I	=	current, A
$[I_C]$	=	moment of inertia matrix, $[3 \times 3]$, kg $\cdot$ m^2
I_{ij}	=	moment of Inertia component, kg $\cdot$ m^2
i, j	=	index parameter
J	=	solar irradiance, W/m^2
Kn	=	Knudsen number
k	=	Boltzmann constant, $1.381 \cdot 10^{-23}$ m$^2 \cdot$ kg $\cdot$ s$^{-2} \cdot$ K^{-1}
L_{ref}	=	reference Length, m
l_i	=	lift angle cosine
$\boldsymbol{m}$	=	magnetic moment, $[3 \times 1]$, (N $\cdot$ m)/T
n	=	number of turns in a wire
$\hat{\boldsymbol{n}}$, $\hat{\boldsymbol{n}}_i$	=	unit normal vector (indexed), $[3 \times 1]$
P	=	solar momentum flux, kg/(m $\cdot$ s^2)
P_{Earth}	=	Earth momentum flux, kg/(m $\cdot$ s^2)
p_s, $p_{s,i}$	=	coefficient of specular reflection (indexed)
R	=	specific gas constant, 8.314 J/K/mol
$\boldsymbol{r}$, $\boldsymbol{r}_i$	=	position vector (indexed), $[3 \times 1]$, m
$\hat{\boldsymbol{r}}_g$	=	unit vector in direction of local gravity, $[3 \times 1]$
$\hat{\boldsymbol{r}}_{\odot}s$	=	unit sun satellite vector, $[3 \times 1]$
$\hat{\boldsymbol{r}}_{?s}$	=	unit Earth satellite vector, $[3 \times 1]$
T	=	temperature, K
$\boldsymbol{T}$	=	torque Vector, $[3 \times 1]$, N $\cdot$ m
$\hat{\boldsymbol{u}}_{L,i}$	=	unit lift vector, $[3 \times 1]$
$\boldsymbol{V}_{\text{atm}}$	=	local atmospheric velocity, $[3 \times 1]$, m/s
$\boldsymbol{V}_{\text{rel}}$	=	velocity relative to atmospheric velocity, $[3 \times 1]$, m/s
$\boldsymbol{V}_{\text{sat}}$	=	satellite velocity, $[3 \times 1]$, m/s
x, y, z	=	coordinates of Reference frame, depends on reference frame
μ	=	standard gravitational parameter (Earth), $3.9860043 \cdot 10^{14}$ m^3/s^2
ρ	=	air density, kg/m^3
$\sigma_{p,\text{abs}}$	=	absolute standard deviation of p, dimension of p
$\sigma_{p,\text{rel}}$	=	relative standard deviation of p
ϕ, θ, ψ	=	roll, pitch, and yaw angle, rad
$\boldsymbol{\omega}$	=	angular velocity, $[3 \times 1]$, rad/s
$\boldsymbol{\omega}_E$	=	rotation rate of the Earth, $[3 \times 1]$, rad/s
$\boldsymbol{\Omega}$	=	angular velocity of a reference frame, $[3 \times 1]$, rad/s

Received 5 June 2018; revision received 18 November 2018; accepted for publication 17 January 2019; published online Open Access 26 February 2019.

*Professor, Space Systems for Planetary Applications Research Team, 10 Ave E. Belin; raphael.garcia@isae supaero.fr.

†Master Student, Space Systems for Planetary Applications Research Team, 10 Ave E. Belin; zimosibbing@gmail.com.

‡Master Student, Space Systems for Planetary Applications Research Team, 10 Ave E. Belin; Adriaen.VAN CAMP@student.isae supaero.fr.

I. Introduction

THE determination of the air density along the track of low Earth orbit (LEO) satellite missions is possible by the recovery of the air drag force and momentum applying on the satellite. The best example of such methods is provided by the GOCE (Gravity field and steady state Ocean Circulation Explorer) space mission [1], which was able to retrieve the air drag force acting on the satellite due to very precise accelerometers and a drag compensation system [2]. From these data, the air density and winds in the thermosphere were inverted along the satellite track [3]. Another way to retrieve the air density is through the drag torque applying on the satellite that changes its rotation rate according to its geometry, orientation, relative air velocity, and the air density. This method was applied successfully to the Venus Express spacecraft and allowed atmospheric density retrieval in the Venus thermosphere [4]. This second method requires the position of the center of application of external surface forces, which is the center of figure (CoF) in our case, to be different from the one of the center of gravity (CoG). This was achieved with the Venus Express spacecraft by rotating one of the two solar panels.

Despite clear demonstrations of the capabilities of such methods to retrieve thermosphere air density, very few space missions investi gated such experiments. For the density retrieval relying on drag force, such experiments are clearly limited by the required noise level on the accelerometer payload, which can be reached only for expensive or dedicated mission platforms. Whereas for the density retrieval relying on drag torque, the uncertainty level required on rotation rate measurements can be reached by most space gyroscopes. However, such experiments are usually not performed for two main reasons. First, the spacecraft is usually designed to have its CoF very

close to its CoG to improve its attitude control. Then, spacecraft missions are usually not operating in the very LEO altitude range (<300 km) because they are passivated before reentry. These limitations do not apply to CubeSat missions that are usually in LEO and are operated until the end of their life.

This study considers the general case of a 3U (three units) CubeSat in LEO that is able to measure its rotation rate, know its attitude control torques, and determine its attitude, either on board or on ground. Such a platform is a NanoSatellite of less than 5 kg and size of $10 \times 10 \times 34$ cm^3 imposed by the CubeSat standards [5]. In a first part, we describe the physics, the system of equations, and the tools set to simulate the it. In a second part, we apply this tool to estimate the air density retrieval capability as a function of various parameters and noise levels, using EntrySat platform as an application case. Then, we conclude on the capability of 3U CubeSats to perform torque experiments and suggest various directions to exploit this capability for future missions.

II. Torques Applying on a Spacecraft

The dynamic torque equation is given by Eq. (1), a combination of equations from [6] (pp. 61, 65), which is valid regardless of the reference system.

$$[I_C]\dot{\boldsymbol{\omega}} + \boldsymbol{\Omega} \times ([I_C]\boldsymbol{\omega}) = \boldsymbol{T} \tag{1}$$

Here, $\boldsymbol{\omega}$ is the angular velocity vector of the rigid satellite body, $[I_C]$ is the MoI matrix, and $\boldsymbol{\Omega}$ is the angular velocity of the trajectory reference frame relative to the inertial reference frame. From [6] (pp. 299 307), we know that the total torque $\boldsymbol{T}$ is the sum of torques from different sources summarized in Eq. (2).

$$\boldsymbol{T} = \boldsymbol{T}_{\text{drag}} + \boldsymbol{T}_{\text{lift}} + \boldsymbol{T}_{\text{gravity}} + \boldsymbol{T}_{\text{SRP}} + \boldsymbol{T}_{\text{albedo}} + \boldsymbol{T}_{\text{res}} + \boldsymbol{T}_{\text{CONTROL}} \tag{2}$$

The terms $\boldsymbol{T}_{\text{drag}}$ and $\boldsymbol{T}_{\text{lift}}$ describe the torques generated by drag and lift surface forces applying on external surfaces of the satellite. Equation systems (3) and (4) are describing these torques.

$$\begin{aligned} \boldsymbol{T}_{\text{drag}} &= \sum_{i\ 1}^{n} \boldsymbol{r}_i \times \boldsymbol{F}_{\text{drag},i} \\ \boldsymbol{F}_{\text{drag},i} &= \frac{1}{2}\rho V_{\text{rel}}^2 C_{D,i} (\hat{\boldsymbol{n}}_i \cdot \hat{\boldsymbol{V}}_{\text{rel}}) A_i (-\hat{\boldsymbol{V}}_{\text{rel}}) \end{aligned} \tag{3}$$

$$\begin{aligned} \boldsymbol{T}_{\text{lift}} &= \sum_{i\ 1}^{n} \boldsymbol{r}_i \times \boldsymbol{F}_{\text{lift},i} \\ \boldsymbol{F}_{\text{lift},i} &= \frac{1}{2}\rho V_{\text{rel}}^2 C_{L,i} (\hat{\boldsymbol{n}}_i \cdot \hat{\boldsymbol{V}}_{\text{rel}}) A_i \hat{\boldsymbol{u}}_{L,i} \end{aligned} \tag{4}$$

where i is the index summing all the aerodynamic panels of the satellite, $\boldsymbol{r}$ the position vector of the center of each aerodynamic panel with respect to the CoG, ρ the atmospheric density, $\boldsymbol{V}_{\text{rel}}$ the velocity of the satellite relative to the atmosphere (V_{rel} denotes the scalar value, $\hat{\boldsymbol{V}}_{\text{rel}}$ denotes the unit dimensionless vector), and $C_{D,i}$, $C_{L,i}$, A_i, $\hat{\boldsymbol{n}}_i$, and $\hat{\boldsymbol{u}}_{L,i}$ are the drag and lift coefficient, area and unit normal and lift direction vectors, of each aerodynamic panel, respectively. The drag and lift coeffi cients are computed according to [7] (pp. 66 71), and take into account the noncontinuum flow regime and the effect of diffusive particle movement. The velocity of the satellite relative to the atmosphere, $\boldsymbol{V}_{\text{rel}}$, depends on the local atmo sphere, which rotates with the Earth, according to [8] (pp. 658). According to works as [6,7], the lift is a negligible force when it comes to aerodynamic torques in space, and we will therefore neglect it in Eq. (2).

The gravity gradient torque $\boldsymbol{T}_{\text{gravity}}$ is given by Eq. (5) ([9] p. 44). We prefer this exact formulation to the more usual formulation from [6] (pp. 299 307), which only takes the diagonal terms of the inertia matrix into account.

$$\boldsymbol{T}_{\text{gravity}} = 3\frac{\mu}{|\boldsymbol{r}|^3}\hat{\boldsymbol{r}}_g \times (I\hat{\boldsymbol{r}}_g) = 3\frac{|\boldsymbol{g}|}{|\boldsymbol{r}|}\hat{\boldsymbol{r}}_g \times (I\hat{\boldsymbol{r}}_g) \tag{5}$$

where $\boldsymbol{\mu}$ is the gravitational parameter, $\boldsymbol{r}$ the radial distance to the center of the Earth, $\hat{\boldsymbol{r}}_g$ the unit vector in direction of the local gravity field, and I_{ii} are elements of moment of inertia (MoI) matrix, with $i \in \{x, y, z\}$. Using Eq. (5), the gravity torque can be determined.

The solar radiation pressure is an external force, which acts on the effective area of the satellite as seen from the solar radiation direction. A torque, $\boldsymbol{T}_{\text{SRP}}$, is exerted as a result, of which the expression is given in Eq. (6), according to [6] (pp. 299 307) and [7] (pp. 57, 64 66):

$$\begin{aligned} \boldsymbol{T}_{\text{SRP}} &= \sum_{i\ 1}^{n} \boldsymbol{r}_i \times \boldsymbol{F}_{\text{SRP},i} \\ \boldsymbol{F}_{\text{SRP},i} &= \boldsymbol{C}_{r,i} A_{\text{ref}} P \\ \boldsymbol{C}_{r,i} &= \begin{cases} 0 & \text{for } \gamma_i \le 0 \\ \left[(1 - p_{s,i} - p_{d,i})\hat{\boldsymbol{r}}_{\odot s} + 2p_{s,i}\gamma_i \hat{\boldsymbol{n}}_i + p_{d,i}(\hat{\boldsymbol{r}}_{\odot s} - \frac{2}{3}\hat{\boldsymbol{n}}_i) \right] \frac{A_i \gamma_i}{A_{\text{ref}}} & \text{for } \gamma_i > 0 \end{cases} \end{aligned} \tag{6}$$

where P is the momentum flux; A_{ref} the frontal reference area; i the index of the satellite face; $p_{s,i}$ and $p_{d,i}$ the coefficients of specular and diffusive reflection, respectively; $\hat{\boldsymbol{r}}_{\odot s}$ the unit vector from the sun to the spacecraft; γ_i the cosine of the incidence angle; $\hat{\boldsymbol{n}}_i$ the normal vector of each surface; and A_i the area of each surface. The coefficients $p_{s,i}$ and $p_{d,i}$ are material properties that could either be obtained through an experiment or estimated using data on the solar arrays of EntrySat. The frontal reference area A_{ref} is calculated through Eq. (7):

$$A_{\text{ref}} = \sum_{i\ 1}^{n} A_i \gamma_i \tag{7}$$

The momentum flux P can be calculated through the solar irradiance J using Eq. (8):

$$P = \frac{J}{c} \tag{8}$$

where c is the speed of light. For data on J, TSI data from [10] are used, which gives the irradiance with a temporal resolution of 6 h.

The Earth albedo torque $\boldsymbol{T}_{\text{albedo}}$ consists of roughly the same elements as the solar radiation pressure torque, because the driving force is radiation, except that sun's radiation is now reflected on the Earth's surface instead of coming from the sun directly. The expression for $\boldsymbol{T}_{\text{albedo}}$ is extracted from [6] (p. 358), and given in Eq. (9):

$$
\begin{aligned}
\boldsymbol{T}_{\text{albedo}} &= \sum_{i\ 1}^{n} \boldsymbol{r}_i \times \boldsymbol{F}_{\text{albedo},i} \\
\boldsymbol{F}_{\text{albedo},i} &= \boldsymbol{C}_{r,i} A_{\text{ref}} P_{\text{Earth}} \\
\boldsymbol{C}_{r,i} &= \begin{cases} 0 & \text{for } \gamma_i \le 0 \\ \left[(1 - p_s - p_d)\hat{\boldsymbol{r}}_{\odot s} + 2p_s\gamma_i\hat{\boldsymbol{n}}_i + p_d\left(\hat{\boldsymbol{r}}_{\odot s} - \frac{2}{3}\hat{\boldsymbol{n}}_i\right)\right]\frac{A_i\gamma_i}{A_{\text{ref}}} & \text{for } \gamma_i > 0 \end{cases} \\
P_{\text{Earth}} &= \frac{1}{c}\text{JaF}
\end{aligned} \tag{9}
$$

with parameters A_i, γ_i, $p_{s,i}$, $p_{d,i}$, and $\hat{\boldsymbol{n}}_i$ defined as in Eq. (6), A_{ref} defined as in Eq. (7), and parameters J and c defined as in Eq. (8). Here, $\hat{\boldsymbol{r}}_{\odot s}$ is the unit vector from the Earth's center to the spacecraft, $a = 0.367$ is the Earth's albedo (from [11] p. 516), and F is the visibility factor. The visibility factor depends on the altitude of the satellite and the angle between the local vertical and the sun's rays on Earth. A graph is shown in [6] (p. 359). However, the accuracy of these values is limited.

This residual magnetic dipole of the spacecraft will exert a torque. This residual dipole, either permanent or induced by currents in the satellite, must be determined by a ground experiment on the fully integrated satellite. As a means of having some value as an input for the model, we use the value $\boldsymbol{m}_{\text{res}} = 0.009\ \text{A/m}^2$ from a 3U CubeSat Space Dart described in [12]. The resulting torque is given by Eq. (10), according to [6] (pp. 299 307):

$$\boldsymbol{T}_{\text{res}} = \boldsymbol{m}_{\text{res}} \times \boldsymbol{B} \tag{10}$$

where $\boldsymbol{B}$ is the local magnetic flux density.

The last term in torque Eq. (2) ($\boldsymbol{T}_{\text{CONTROL}}$) is the torque exerted by the attitude control system of the satellite to orient itself in space. This torque is assumed to be known from housekeeping parameters of the satellite. In our example, a 3U CubeSat, magneto torquer subsystems are often used to perform attitude control. In this particular case, $\boldsymbol{T}_{\text{CONTROL}}$ is provided by the following equation:

$$\boldsymbol{T}_{\text{CONTROL}} = \boldsymbol{T}_{\text{MTQ}} = \boldsymbol{m}_{\text{MTQ}} \times \boldsymbol{B} = nIA_c(\hat{\boldsymbol{c}} \times \boldsymbol{B}) \tag{11}$$

where $\boldsymbol{B}$ is defined as in Eq. (10). Either the magnetic moment, $\boldsymbol{m}_{\text{MTQ}}$, can be substituted directly or the expression on the right hand side can be used. Here, n is the number of turns of a wire, I is the current, A_c is the cross sectional area of the coil, and $\hat{\boldsymbol{c}}$ is the unit vector in the direction of the coil axis.

III. Parameters and Simulation Tool

A. Dynamic System Parameters

To perform a numerical simulation of a torque experiment, many input parameters of Eq. (1) should be provided. These parameters will be separated into three different types and described in the next sections: satellite properties, environment parameters (atmosphere, space), and orbit/attitude parameters.

1. *Satellite Properties*

We will consider a typical 3U CubeSat for which construction inaccuracies on parameters such as face areas are negligible. Such platforms have a size of $10 \times 10 \times 34\ \text{cm}^3$ and respect the CubeSat standard format. The center of mass (CoG for center of gravity) will be shifted relative to the CoF along the elongated direction of the satellite. This shift is fixed in these simulations to 2 cm. However, the torques applying on the satellite depend almost linearly on the distance between CoG and CoF, and for a 3U CubeSat involving deployable solar panels this distance may reach values as high as 10 to 20 cm. The MoI values are chosen according to the mechanical model of the EntrySat satellite that has a mass of 2.3 kg. This mass is in the lower range of masses usual for 3U CubeSats (typically up to 4.5 kg). Extension to different satellite masses is somehow straightforward because the inertia is depending linearly on mass. The satellite is also assumed to be able to measure the magnetic field ($\boldsymbol{B}$), its own angular velocity ($\boldsymbol{\omega}$), and consequently the acceleration of this velocity ($\dot{\boldsymbol{\omega}}$) through specific sensors, but also to know the control torques applied by the attitude control subsystem ($\boldsymbol{T}_{\text{CONTROL}}$). Finally, the mission is assumed to be able to determine the satellite orbit and attitude, either on board or on ground. All these parameters will have error bars that depend on the hardware used and on the mission characteristics.

However, the analysis presented below depends only on these assumptions that allows to invert Eq. (1) in order to retrieve drag torque and then air density. Even if a magnetic attitude control, similar to EntrySat mission, is considered here, the capability to retrieve air density does not depend on the type of attitude control (magnetic, reaction wheels, etc.) or on the attitude control scheme (rate reduction mode, pointing in a direction, or no control at all). Only precise estimates of orbit, attitude, and control torque are needed.

2. *Satellite Orbit and Attitudes*

To illustrate a typical case and to cover a broad latitude range, a circular sun synchronous orbit (98.18° inclination) is chosen, and the average altitude is set by fixing the semimajor axis. Three different satellite attitude cases are considered:

1) Attitude model 1 assumes a small face of the satellite perpendicular to the track direction.

2) Attitude model 2 assumes a long face of the satellite perpendicular to the track direction.

3) Attitude model 3 assumes a tumbling attitude evolving according to Eq. (1) without any control ($\boldsymbol{T}_{\text{CONTROL}} = 0$).

The test attitudes 1 and 2 are illustrated in Fig. 1. Drag effects are smaller for attitude 1 model than for attitude 2 model because the area perpendicular to the track direction in attitude 1 model is one third of the area in attitude 2 model. Attitude models 1 and 2 are idealized situations in which the satellite control torque is assumed to compensate exactly all the torques applying on the satellite. These idealized models are used to illustrate the two extreme cases in terms of drag torque effects.

3. *Satellite Environment*

The atmospheric model parameters (air density, temperature, and composition) are extracted from the NRLMSISE 00 model [13]. The gravity field values are extracted from the EGM2008 model. The magnetic field values are extracted from the IGRF model using the magnetic field calculator [14]. The solar radiation pressure parameters are computed by using TSI data from [10], which gives the irradiance with a temporal resolution of 6 h. A single atmosphere model was tested with a conditions corresponding to January 1, 2016, at midnight (solar flux F10.7 of 90.3). The atmospheric state is varying significantly as a function of season and solar cycle. These variations will be investigated in further studies.

B. Simulation Tool

The simulation tool was developed using MATLAB/SIMULINK and makes an extensive use of the aerodynamics toolbox. All the

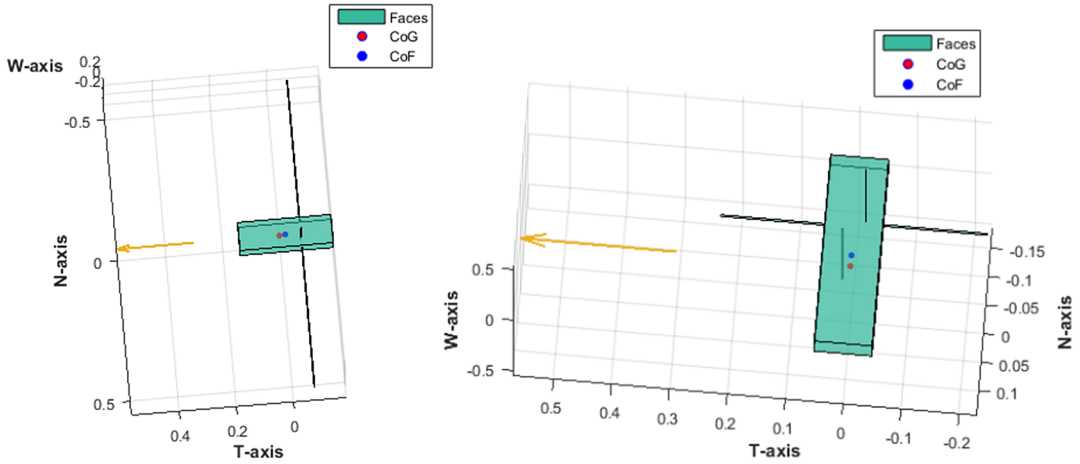

Fig. 1 3U CubeSat satellite in the TNW reference frame for test attitudes 1 (left) and 2 (right).

SIMULINK blocks and MATLAB routines developed outside of the toolboxes have been intensively tested and validated relative to analytical results (not shown). In addition to the parameters presented above, the simulation tool uses a date to extract the satellite environ ment parameters and a time step for the time evolution along the orbit. At each time step the simulation tool passes through the following computations:

1) Propagation of the orbit and update of the attitude according to the attitude model chosen.

2) Computation of "error free" and "data like" (including errors) rotation speeds and torques applying to the satellite according to environment parameters at new position and attitude, and random errors.

3) Inversion of the dynamic torque Eq. (1) in order to retrieve "error free" and "data like" estimates of drag torque $\boldsymbol{T}_{\text{drag,inv}}$. In this process, if attitude model is 1 or 2, $\boldsymbol{T}_{\text{CONTROL}}$ is set to cancel error free torques in order to keep a constant attitude (in TNW frame), whereas it is set to zero for attitude model 3.

4) Air density recovery from "data like" values of drag torque $\boldsymbol{T}_{\text{drag,inv}}$, satellite attitude and environment parameters.

5) If attitude model is 3, propagation of the satellite attitude by integrating the "error free" dynamic Eq. (1).

The split of computations in "error free" and "data like" branches allow to both propagate consistently the dynamic attitude evolution and to estimate the effects of various errors in the system. The type satellite control is not important as soon as we know the attitude and the control torques of the satellite and their associated error bars. The air density is estimated at each step by inversion of Eq. (1) with "data like" parameters including errors. This is a worse case method for performing this inversion because any data filtering or a priori assumption added to the inversion process would improve the results.

C. Magnitudes of Torques Applied on a 3U CubeSat

Before starting the complex analysis, we present in Fig. 2 the magnitudes of the different torques as a function of altitude along a sun synchronous orbit. A few interesting features can be observed. First, the Earth's albedo and solar radiation torques appear to be negligible relative to other torques. Then, in this worst case hypo thesis for the satellite magnetic moment, the torque induced by the residual magnetic moment is overpassing the gravity gradient torque by one order of magnitude. This observation suggests that missions relying on gravity gradient torque stabilization should take care of the residual magnetic moment of the satellite. Depending on the attitude of the satellite, the drag torque is dominant below 250 300 km. Moreover, it is higher than the maximum attitude control torque that can be exerted by a typical magneto torquer below 200 or 140 km depending on the satellite attitude. This means that in this altitude range the satellite is not able to control its attitude anymore. This situation is not affecting our capability to recover the air density as far as the satellite is rotating slowly enough to be able to recover precisely its attitude and the control torques are known. The difference between the drag torques of the two attitude models is more than the difference of area facing the flow because the CoG shift is set in the direction of the long face of the satellite, further increasing the torque when the long face is facing the flow. All these results suggest that the drag torque is dominating below 200 300 km altitude and that the air density can be retrieved in this range.

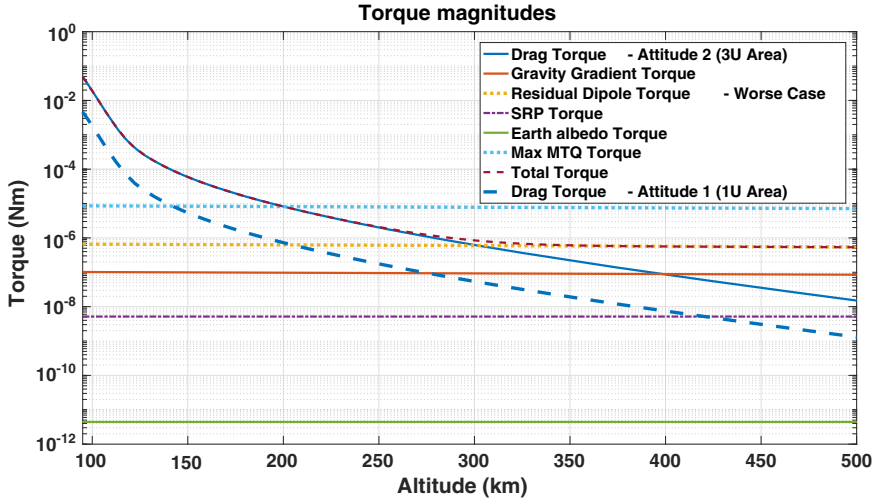

Fig. 2 Magnitude of torques applying on a 3U CubeSat as a function of altitude for the two extreme attitude situations (models 1 and 2).

IV. Air Density Retrieval: Numerical Experiments

A. An Application Case: The EntrySat Mission

To be fully representative of a CubeSat mission, the simulation tool requires a lot of details on the uncertainty of the parameters. In addition, the parameter space is so large that it is difficult to infer the effect of variation in these parameters without having some realistic a priori values. That is why we choose to apply the simulation tool to a real CubeSat mission: the EntrySat project.

The primary science objective of EntrySat is to constrain the reentry of space debris by measuring the following parameters during the last tens of orbit in the satellite life (altitude below 170 km height):

1) Heat flux, external temperature, and pressure applied on five of the six faces of the satellite

2) Accelerations and rotations of the satellite

3) Position of the satellite

The first set of measurements is performed by external sensors from which the data are collected by an homemade sensor board. These measurements are not considered in this study. The accele rations and rotations of the satellite are measured by ADIS16485 inertial measurement unit (IMU) from analog device company. The positions are acquired by OEM615 single frequency GPS receiver from Novatel company.

A secondary science objective is to perform air density retrieval with a torque experiment during the orbital phase of the mission at various altitudes. To do so, in addition to the measurements described above, we will use measurements of magnetic field and coil currents in iMTQ magneto torquer from ISIS company. Satellite attitude is not controlled; however, the magneto torquer will be used in rate reduction mode to reduce the rotation speed of the satellite. This situation is not impacting our capability to perform torque retrieval if we are able to know the torques applied by the magneto torquer, and to reconstruct precisely enough the attitude of the spacecraft on the ground. For this task, we will use gyroscopes, magnetic field measurements, and heat flux sensors that are acting as sun sensors when illuminated. Satellite is operated from ISAE SUPAERO through VHF/UHF communication, and the data acquired during reentry phase (last day of satellite life) will be send back through iridium satellite to satellite communication.

EntrySat platform is fully space qualified and will be launched by the NanoRacks company to the international space station in spring 2019, and released from the Space Station. Figure 3 provides views of the satellite presenting the subsystem elements and the mechanical accommodation.

B. Errors on Data and Parameters

As already described above, our tool allows to insert random errors on various parameters. We have inserted typical errors on all the parameters that were extracted from data sheets of the materials used in our CubeSat project EntrySat, from values obtained by tests in the framework of EntrySat project, or from the references described in Sec. II. These error levels are presented in Table 1, and are used to construct Gaussian random variables, which are added into the simulation tool. The errors on the control torque are taken into account by the error bar on the estimate of the magnetic moment generated the magneto torquer (last line of the table). The magnetic measurements performed by magneto torquer subsystem are not influenced by the magnetic control because these measurements are performed only when the temperature of the satellite surface is needed for the computation of drag and radiation pressure coeffi cients. The small error presented for the drag coefficient is coming only from the error on the material properties. However, the errors on the spacecraft attitude and, to a less extent, air temperature propagate into drag coefficient estimates, thus generating variations much larger than 1%. The residual magnetic dipole has been determined by magnetic test performed on EntrySat flight model (about 20 $\text{mA} \cdot \text{m}^2$). Its value does not vary by more than 4 $\text{mA} \cdot \text{m}^2$ with the satellite operation mode, and variations within a given mode remains below the uncertainty of the magnetic test facility (about 0.4 $\text{mA} \cdot \text{m}^2$).

Table 1 Error budget for the simulation tool

Category	Source (variable)	σ_p
	General	
Orbit	Position ($\boldsymbol{r}$)	(100, 100, 100) m
Attitude	Accuracy	(0.68, 0.58, 0.68) deg
Attitude	Angular velocity ($\boldsymbol{\omega}$)	(20, 20, 20) deg /h
Attitude	Angular acceleration ($\dot{\boldsymbol{\omega}}$)	$(1, 1, 1)\ 10^{-5}$ rad/s^2
Satellite	Center of gravity ($\boldsymbol{r}_i$)	(0, 0, 1) mm
Satellite	Moment of inertia ($[I_C]$)	0.1% [3 × 3]
	Torque sources	
Drag	Air relative velocity ($\boldsymbol{V}_{\text{rel}}$)	(100, 100, 100) m/s
Drag	Drag coefficient (C_D)	1%
Drag	Temperature (T)	14 K
SRP	Solar momentum flux (P)	10^{-9} kg/ms^2
SRP	Coefficient of specular reflection ($p_{s,i}$)	0.0005
SRP	Coefficient of diffusive reflection ($p_{d,i}$)	0.003
SRP	Radiation pressure coefficient ($\boldsymbol{C}_{\text{SRP}}$)	1%
Earth albedo	Visibility factor (F)	20%
Earth albedo	Radiation pressure coefficient ($\boldsymbol{C}_{\text{EA}}$)	1%
Residual dipole	Residual dipole ($\boldsymbol{m}_{\text{res}}$)	$(40, 6, 6)\ 10^{-5}$ Am^2
Magnetic measurements	Magnetometer ($\boldsymbol{B}$)	(500, 500, 500) nT
	Control	
MTQ	Accuracy ($\boldsymbol{m}_{\text{MTQ}}$)	$(1, 1, 0.4)\ 10^{-2}$ Am^2

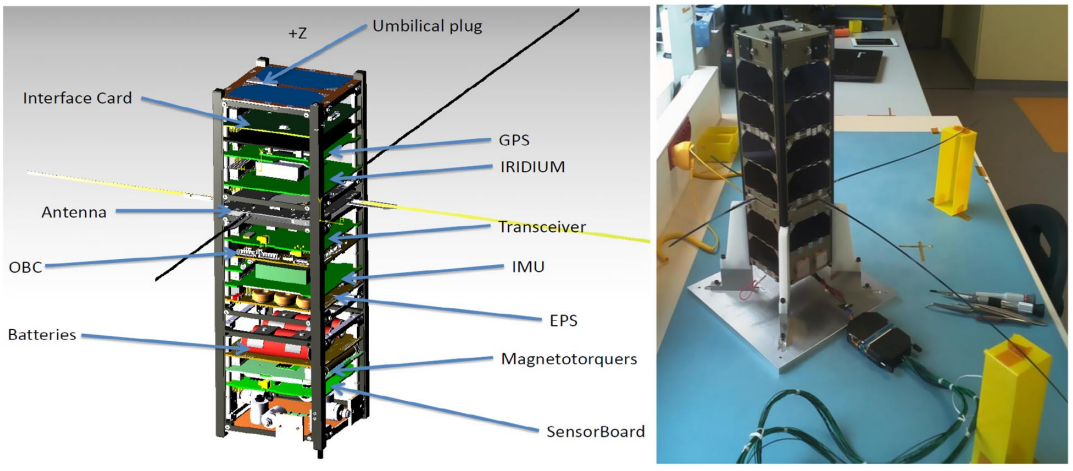

Fig. 3 Description of EntrySat 3U CubeSat platform. On the left, drawing presenting the subsystem elements. On the right, picture of the flight model with antenna system opened. Note that satellite orientation is reserved on the two pictures.

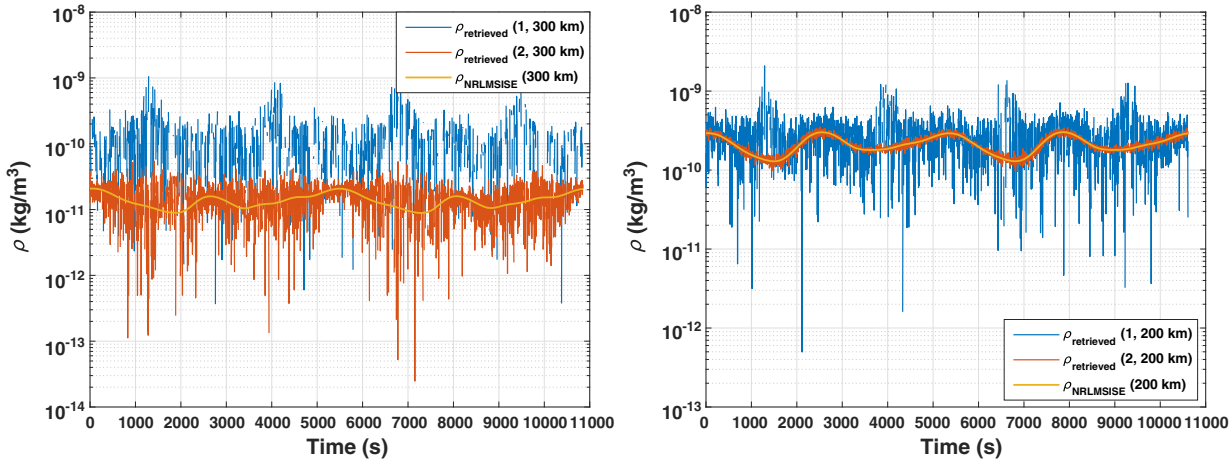

Fig. 4 The theoretical density and the retrieved density outputs of our simulation tools for sun-synchronous orbits at altitudes 300 km (left) and 200 km (right), and test attitudes 1 (1U facing flow) and 2 (3U facing flow).

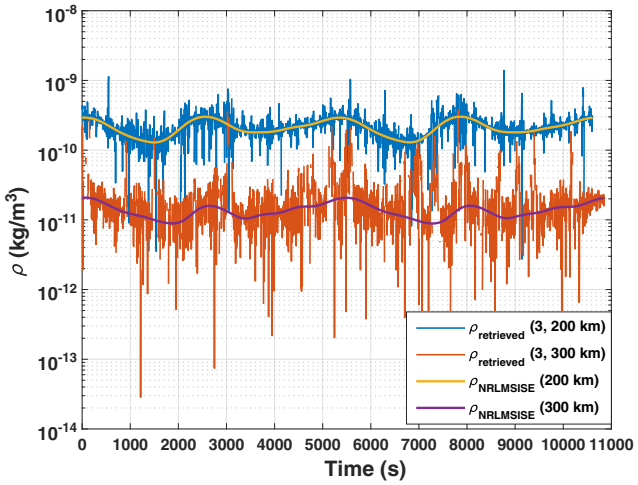

Fig. 5 The theoretical density and the retrieved density outputs of our simulation tools for sun-synchronous orbits at altitudes 300 and 200 km for an attitude model 3 (uncontrolled attitude).

Consequently, a constant value of 20 mA $\cdot$ m^2 is imposed in the simulation tool and variations are restricted within 0.4 mA $\cdot$ m^2.

C. Examples of Air Density Retrieval

Figure 4 gives examples of air density retrieval by our tool. Attitude models 1 and 2 are tested for orbit altitudes of 300 and 200 km. The most favorable attitude model (2), which is presenting a 3U face to the flow, allows to recover the air density at 200 km altitude properly, but other situations are presenting estimates far away from the input air density.

Another air density retrieval example is provided in Fig. 5 with attitude model 3 assuming that the spacecraft attitude is not controlled. This case provides results in between the results of attitude models 1 and 2, but suggests that air densities can be retrieved close to 200 km altitude.

These results were obtained assuming that all error levels listed in Table 1 were simultaneously acting on the air density estimates. The influence of particular error sources is considered in the next section.

The capability of our method to recover neutral density at about 200 km altitude is difficult to compare with other methods because

Table 2 Effects of various error sources on the absolute and relative air density retrievals in polar and equatorial regions with attitude model 1

Source (variable)	$\sigma_p(x)$, $\sigma_p(y)$, $\sigma_p(z)$	$\sigma_{\rho,\text{abs}}$	$\sigma_{\rho,\text{rel}}$	$\sigma_{\rho,\text{abs}}$	$\sigma_{\rho,\text{rel}}$
		Polar		Equatorial	
		General			
Position ($\boldsymbol{r}$)	(100, 100, 100) m	2.54 10^{-13}	0.00155	5.44 10^{-13}	0.00190
Attitude Accuracy	(0.68, 0.58, 0.68) deg	1.57 10^{-10}	0.984	3.19 10^{-11}	0.112
Angular velocity ($\boldsymbol{\omega}$)	(20, 20, 20) deg /h	3.22 10^{-12}	0.0207	9.74 10^{-14}	0.000341
Angular acceleration ($\dot{\boldsymbol{\omega}}$)	(1, 1, 1) 10^{-5} rad/s^2	2.12 10^{-10}	1.37	7.20 10^{-11}	0.253
Center of gravity ($\boldsymbol{r}_i$)	(0, 0, 1) mm	9.21 10^{-13}	0.00563	2.93 10^{-12}	0.0103
Moment of inertia ($[I_C]$)	0.1% [3 × 3]	2.46 10^{-14}	0.000149	2.79 10^{-16}	9.82 10^{-7}
		Torque sources			
Air relative velocity ($\boldsymbol{V}_{\text{rel}}$)	(100, 100, 100) m/s	1.88 10^{-10}	1.15	3.84 10^{-11}	0.134
Drag coefficient (C_D)	1%	1.97 10^{-12}	0.0121	4.33 10^{-12}	0.0151
Temperature (T)	14 K	2.15 10^{-13}	0.00129	5.07 10^{-13}	0.00177
Solar momentum flux (P)	10^{-9} kg/ms^2	1.11 10^{-15}	7.30 10^{-6}	4.04 10^{-16}	1.42 10^{-6}
Coefficient of specular Refl. (p_s)	0.0005	8.01 10^{-16}	4.33 10^{-6}	5.79 10^{-16}	2.04 10^{-6}
Coefficient of diffusive refl. (p_d)	0.003	3.99 10^{-15}	2.13 10^{-5}	1.35 10^{-15}	4.75 10^{-6}
Radiation pressure coefficient ($\boldsymbol{C}_{\text{SRP}}$)	1%	2.89 10^{-14}	1.55 10^{-4}	1.13 10^{-14}	3.96 10^{-5}
Visibility factor (F)	20%	8.77 10^{-14}	4.73 10^{-4}	3.01 10^{-15}	1.08 10^{-5}
Radiation pressure coefficient ($\boldsymbol{C}_{\text{EA}}$)	1%	4.81 10^{-15}	2.60 10^{-5}	1.08 10^{-16}	3.85 10^{-7}
Residual dipole ($\boldsymbol{m}_{\text{res}}$)	(40, 6, 6) 10^{-5} Am^2	3.39 10^{-12}	0.0228	3.67 10^{-12}	0.0128
Magnetometer ($\boldsymbol{B}$)	(500, 500, 500) nT	1.31 10^{-11}	0.0891	1.67 10^{-12}	0.00588
		Control			
MTQ accuracy ($\boldsymbol{m}_{\text{MTQ}}$)	(1, 1, 0.4) 10^{-2} Am^2	2.20 10^{-10}	1.50	8.89 10^{-11}	0.309
All errors		4.57 $\mathbf{10^{-10}}$	2.95	1.26 $\mathbf{10^{-10}}$	0.440

Table 3 Effects of various error sources on the relative air density retrievals in equatorial regions at 200 km altitude for different attitude models

Source (variable)	$\sigma_p(x)$, $\sigma_p(y)$, $\sigma_p(z)$	$\sigma_{\rho,\mathrm{rel}}$ Attitude 1	$\sigma_{\rho,\mathrm{rel}}$ Attitude 2	$\sigma_{\rho,\mathrm{rel}}$ Attitude 3
	General			
Position ($\boldsymbol{r}$)	(100, 100, 100) m	0.00190	0.00189	0.00189
Attitude accuracy	(0.68, 0.58, 0.68) deg	0.112	0.0264	0.109
Center of gravity ($\boldsymbol{r}_i$)	(0, 0, 1) mm	0.0103	0.0494	0.0236
Air relative velocity ($\boldsymbol{V}_{\mathrm{rel}}$)	(100, 100, 100) m/s	0.134	0.0391	0.133
Drag coefficient (C_D)	1%	0.0151	0.00962	0.0332
Residual dipole ($\boldsymbol{m}_{\mathrm{res}}$)	(40, 6, 6) 10^{-5} Am^2	0.0128	5.77 10^{-4}	0.00838
MTQ accuracy ($\boldsymbol{m}_{\mathrm{MTQ}}$)	(1, 1, 0.4) 10^{-2} Am^2	0.309	0.0165	0.252
All errors		0.440	0.0717	0.317

the results depend strongly on the atmospheric state, the quality of on board instruments, and the mission design. Moreover, methods relying on drag forces and torques applying on the satellite have the capability to infer high frequency variations along the orbit that methods relying on orbit variation are averaging out. A review covering all the methods to recover thermosphere neutral density is presented by [15]. However, this study does not cover retrieval by estimation of drag torque. To have a comparison between capabilities of neutral density estimate by estimation of drag force and drag torque on the same mission, we should go to the analysis of Venus Express aerobreaking phases [4]. This study demonstrates that neutral density estimates with drag torque method can provide reliable results at altitudes 50 km larger than the ones obtained from methods relying on drag force.

D. Error Analysis

To understand what the dominating error sources are for air density retrieval, error sources were injected one by one in the simulation tool, and the standard deviation of the relative air density misfit was computed. Table 2 presents the whole computation for the attitude model 1 case at 200 km altitude. Results are presented along polar and equatorial arcs, because air density and magnetic conditions are different in these two regions. The results presented here are consistent with the ones observed in the previous section, with equatorial regions better constrained than polar regions, and large errors in this particular case. It is also clear that all radiation parameters have a very weak influence due to the relatively small induced torques. The dominating error sources appear to be linked to the measurements or modeling of the dynamics of the satellite (attitude knowledge, angular acceleration, relative air velocity), but also to magnetic parameters (precision on residual magnetic dipole, magnetic field measurement on board). Such a table allows to compute rough linear sensitivities of air density errors induced by the errors on the related parameters.

Table 3 presents the effects of the main error drivers on air density retrieval for the three different attitude models at 200 km altitude along equatorial orbit arcs. The error on the residual magnetic dipole determination is dominant in most cases, despite the fact that the analysis is performed along equatorial arcs. However, the value of this error is probably overestimated by a factor 5 from tests we performed during the EntrySat project in a nonmagnetic chamber. Another important error source comes from winds in the thermosphere that induce 3 to 13% error levels. The knowledge of the satellite attitude also appears to be critical, because even a knowledge at 1° level is generating errors reaching 10% on the air density retrieval. Finally, it is also worth to note that a 1 mm error on the position of the center of mass of the satellite can generate error levels on air density retrieval reaching 5%.

The case of uncontrolled attitude (attitude model 3) appears to be in between the best and worst attitude cases, suggesting that the air density retrieval is possible as soon as the attitude is precisely reconstructed.

V. Conclusions

The dynamic torque model created to analyze the capability of 3U CubeSats to infer thermosphere air density allows to demonstrate the following points. Air density retrieval may be possible below 250 km altitude for realistic estimates of error bars applying to CubeSat equipment, sensors, positioning, and attitude control subsystems. Such an experiment does not require to precise attitude control, but requires precise determination of the satellite orientation and rotation parameters. Precise determination of the satellite residual magnetic dipole and center of mass position is required before launch to ensure a proper air density retrieval. The sensitivity to drag is strongly dependent on the spacecraft shape, distance between center of gravity and center of figure, and attitude. The winds in the thermosphere also appear to have a significant impact on air density retrieval.

The simulation tool developed in this study can be adapted to infer quickly the capability of ongoing or projected CubeSat missions to perform such air density retrieval. In addition, it will be applied to the data analysis of the EntrySat 3U CubeSat, for which such an experi ment is foreseen. The capability of doing such experiments with low cost platforms such as CubeSats opens the way to new observations of the thermosphere density space and time variations. Such obser vations are critical to understand interactions between the thermo sphere dynamics and external and lower atmosphere forcing sources.

Acknowledgments

CNES funded EntrySat CubeSat in the framework of JANUS student satellite projects. Zimo R. Sibbing was funded by the Erasmus European student exchange program during his stay at ISAE SUPAERO. We thank Eelco Doornbos (TU Delft) for stimulating discussions and exchanges of students.

References

[1] Romanazzo, S. C. M., Sechi, G., Saponara, M., Rezazad, M., Piris Nino, A., Da Costa, A., Fehringer, M., Floberghagen, R., Andre, G., and Emanuelli, P., "In Orbit Experience with the Drag Free Attitude and Orbit Control System of ESA's Gravity Mission GOCE," *GNC 2011: 8th International ESA Conference on Guidance, Navigation and Control Systems*, ESA, Noordwijk, The Netherlands, 2011, pp. 1 17.

[2] Floberghagen, R., Fehringer, M., Lamarre, D., Muzi, D., Frommknecht, B., Steiger, C., Piñeiro, J., and da Costa, A., "Mission Design, Operation and Exploitation of the Gravity Field and Steady State Ocean Circulation Explorer Mission," *Journal of Geodesy*, Vol. 85, No. 11, 2011, pp. 749 758. doi:10.1007/s00190 011 0498 3

[3] Doornbos, E., van den IJssel, J., Luehr, H., Foerster, M., Koppenwallner, G., Bruinsma, S., Sutton, E., Forbes, J. M., Marcos, F., and Perosanz, F., "Neutral Density and Crosswind Determination from Arbitrarily Oriented Multiaxis Accelerometers on Satellites," *Journal of Spacecraft and Rockets*, Vol. 47, No. 4, 2010, pp. 580 589. doi:10.2514/1.48114

[4] Persson, M., "Venus Thermosphere Densities as Revealed by Venus Express Torque and Accelerometer Data," 2015, %http://www.diva portal. org/smash/record.jsf?pid diva2%3A1021822&dswid 7265.

[5] Pignatelli, D., and Mehrparvar, A., "CubeSat Design Specifications Rev. 13," *The CubeSat Program, Cal Poly SLO*, California Polytechnic State Univ., San Luis Obispo, CA, 2013.

[6] Fortescue, P., Swinerd, G., and Stark, J., *Spacecraft Systems Engineering*, Wiley, Chichester, United Kingdom, March 2011, p. 704, http://adsabs.harvard.edu/abs/2003sse..book.....F.

[7] Doornbos, E., *Thermospheric Density and Wind Determination from Satellite Dynamics*, Springer Verlag, Berlin, 2012, p. 181.

[8] Curtis, H., *Orbital Mechanics for Engineering Students*, Butterworth Heinemann, Oxford, United Kingdom, 2013, p. 750.

[9] CNES, *Techniques et Technologies des Véhicules Spatiaux*, Centre National d'Études Spatial, 2015.

[10] LISIRD, "Total Solar Irradiance (TSI) Measurements," 2016, http://lasp.colorado.edu/lisird/tsi/.

[11] Lissauer, J. J., and de Pater, I., *Fundamental Planetary Science: Physics, Chemistry and Habitability*, Cambridge Univ. Press, New York, 2013, p. 583.

[12] Armstrong, J., Casey, C., Creamer, G., and Dutchover, G., "Pointing Control for Low Altitude Triple CubeSat Space Darts," *Proceedings of the 23rd Annual AIAA/USU Conference on Small Satellites*, Bepress, Berkeley, 2009.

[13] Picone, J. M., Hedin, A. E., Drob, D. P., and Aikin, A. C., "NRLMSISE 00 Empirical Model of the Atmosphere: Statistical Comparisons and Scientific Issues," *Journal of Geophysical Research (Space Physics)*, Vol. 107, No. A12, Dec. 2002, pp. SIA 15 1 SIA 15 16. doi:10.1029/2002JA009430

[14] NOAA, "Magnetic Field Calculators," 2016, http://www.ngdc.noaa.gov/geomag web/#igrfgrid.

[15] Emmert, J. T., "Thermospheric Mass Density: A Review," *Advances in Space Research*, Vol. 56, No. 5, 2015, pp. 773 824. doi:10.1016/j.asr.2015.05.038

V. J. Lappas
Associate Editor